Physica A 582 (2021) 126243

Contents lists available at ScienceDirect

Physica A

journal homepage: www.elsevier.com/locate/physa

Modeling the temperature of maximum density of aqueous tert-butanol solutions

Murilo S. Marques [a,b,*], Enrique Lomba [c], Eva G. Noya [c], Diego González-Salgado [d], Marcia Barbosa [b]

[a] Centro das Ciências Exatas e das Tecnologias, Universidade Federal do Oeste da Bahia, Rua Bertioga, 892, Morada Nobre, CEP 47810-059, Barreiras-BA, Brazil
[b] Instituto de Física, Universidade Federal do Rio Grande do Sul, Av. Bento Gonçalves 9500, Caixa Postal 15051, CEP 91501-970, Porto Alegre - RS, Brazil
[c] Instituto de Química Física Rocasolano, CSIC, Calle Serrano 119, E-28006 Madrid, Spain
[d] Departamento de Física Aplicada, Universidad de Vigo, Campus del Agua, Edificio Manuel Martínez-Risco, E-32004 Ourense, Spain

ARTICLE INFO

Article history:
Received 23 February 2021
Received in revised form 21 May 2021
Available online 9 July 2021

Keywords:
Alcohol solutions
Thermodynamic anomalies
Three-body interactions
Molecular dynamics
TMD

ABSTRACT

Short-chain alcohols at high dilution are among the very few solutes that enhance the anomalous behavior of water, in particular the value of the temperature of maximum density. This peculiar feature, first discovered experimentally in the early twenties, has remained elusive to a full explanation in terms of atomistic models. In this paper, we first introduce a two-site model of tert-butanol in which the interactions involving hydrogen bonding are represented by a Stillinger–Weber potential, following the ideas established by Molinero and Moore (2009) for water. Our model parameters are fit so as to semi-quantitatively reproduce the experimental densities and vaporization enthalpies of previously proposed united atom and all atom OPLS models. Water is represented using the aforementioned potential model introduced by Molinero and Moore, with cross interaction parameters between water and tert-butanol optimized to yield a reasonable description of the experimental excess enthalpies and volumes over the whole composition range of the mixture. We will see that our simple model is able to reproduce the presence of a maximum in the change of the temperature of maximum density for very low alcohol mole fractions, followed by a considerable decrease until the density anomaly itself disappears. We have correlated this behavior with changes in the local structure of water and compared it with the results of all-atom simulations of water/tert-butanol mixtures.

1. Introduction

Almost one hundred years ago, Tafell [1] identified an anomalous increase in the temperature of maximum density of water when small amounts of ethanol were added. After four decades, Wada and Umeda carried a rather extensive analysis on the influence of a variety of solutes on this water anomaly [2,3] and found that not only ethanol, but a whole series of highly dilute short chain alcohol solutions exhibit a small rise in the temperature of maximum density. Other polar and apolar solutes, on the contrary, always induce a monotonous decrease of the temperature of maximum density.

* Corresponding author at: Instituto de Física, Universidade Federal do Rio Grande do Sul, Av. Bento Gonçalves 9500, Caixa Postal 15051, CEP 91501-970, Porto Alegre - RS, Brazil.
E-mail address: murilo.sodre@ufob.edu.br (M.S. Marques).

https://doi.org/10.1016/j.physa.2021.126243
0378-4371/

The thermodynamic anomalies of alcohol–water mixtures can be traced back to the corresponding anomalies of pure water [4,5]. Of special relevance is the volume contraction of pure water that occurs with increasing temperature until a maximum density is reached around 4 °C along the atmospheric pressure isobar. The existence of this temperature of maximum density (TMD) is probably the best known singularity of water, studied already since the 17th century [6]. Its microscopic origin is based on the prevalence of the formation of low-density ice-type structures over the high-density close-packed configurations right after melting.

On the other hand, the peculiar response of water properties to the addition of small amounts of solutes has been known for quite some time. Great relevance has been given to the large hydration heat capacities of nonpolar solutes [7]. This is behind the so-called "hydrophobic effect" which is key to biological phenomena of huge importance such as protein folding. Adding small amounts of non-polar solutes to water leads to a considerable increase in the enthalpy, which is compensated by a negative hydration entropy. This balance explains the low solubility of apolar substances in water. Nonetheless, it is quite puzzling why enthalpy should increase upon the addition of negligible quantities of non-polar solutes. Frank and Evans [8] were the first to propose an answer to this question in terms of their "iceberg model". According to their picture, the presence of a hydrophobic solute would induce the reorganization of the surrounding water molecules with an ice-like structure, which in turn would imply an enhancement of the water anomalies (e.g. a rise in the TMD). Being more "ice-like" would also imply a stronger hydrogen bond network, and hence a higher enthalpy. These solutes were originally termed "structure makers", in contrast with those that tend to destroy ice-like structures (e.g. hydrophilic groups), termed "structure breakers" [9,10]. Among other works the simulation study of Galamba [11] partially supports the structural view of the "iceberg model". Quite recently, Ashbaugh and Bukanan [7] provided a detailed account of the effects of hydrophobic hydration on the thermodynamics of non-polar solutes in water, based on extensive molecular dynamics simulations. Their results, which confirm the interplay between enthalpic and entropic effects in the hydration process, indicate that one is to expect a decrease in the TMD of water upon addition of non-polar solutes. According to their analysis, this trend can be reversed at very high pressures but, to the best of our knowledge, this has not been experimentally confirmed as yet. These conclusions seem to contradict the experimental study of Bignell [12], in which the molar volume, v_a, of N_2, O_2 and Ar in aqueous solution at different temperatures was measured. At constant pressure and in the limit of infinite dilution a $\partial v_a/\partial T < 0$ would lead to a rising TMD [7]. This seems to be the case for Ar and other gases in Ref. [12], but only when the data are corrected for the drop in gas solubility due to the increase in temperature. Whether the discrepancy between experiment and simulation is due to a short-coming of the model used in [7] or stems from the data analysis in [12] is unclear to us. In any case, both studies conclude that at least under certain circumstances one should expect a rising TMD in water due to the presence of apolar solutes. The van der Waals type analysis of Chaterjee et al. [13] also indicates that one should expect the TMD to rise with increasing hydrophobicity of the solute, from a practical standpoint the size of its non-polar component. This would seem to agree with the trends observed by Wada and Umeda for short-chain alcohols in water at high dilution [2]. They found that the largest increase in the TMD corresponds to tert-butanol, which is the alcohol with the bulkiest alkyl group that remains soluble in water for all the composition range [14]. The problems raised when analyzing the effects of non-polar solutes in water due to their very low solubility, are circumvented by the presence of the hydroxyl group in alcohol molecules. Since the investigations of Wada and Umeda, a large number of works have addressed the issue of the solute's influence on the TMD of water in the case of short chain alcohols [13,15–21]. Along the lines of the model of Chatterjee et al. [13], Su et al. [19] later proposed a simplified dimer model where the effect of hydrogen bonding is modeled with a two scale potential. In this case, the presence of the solute decreases the TMD. In contrast, another two-length scale potential dimer model proposed in Ref. [21] displayed a behavior in accordance with the experimental data, but for artificially low densities. Interestingly, recent works using full scale atomistic simulations using either united atom OPLS models (see Ref. [20] for methanol/water solutions), or flexible all-atom models (cf. Ref. [22] for methanol, ethanol, propanol, and tert-butanol solutions in TIP4P/2005f water [23]), show that these models fail to reproduce the enhancement of the density anomaly experimentally found for small alcohol concentrations. In all instances the presence of alcohol molecules induces a substantial decrease of the TMD (up to five times larger than the experimental one for concentrations $x_{R-OH} \sim 0.01$).

From the experimental standpoint, there is a growing evidence that at low concentrations, the hydrophobic hydration of the alkyl groups in alcohols induces a stiffening of the hydrogen bond network, which is likely connected with the enhancement of the anomalous behavior of their dilute solutions. This has been confirmed by compressibility and sound speed data [24], femtosecond infrared spectroscopy [25], Raman scattering multivariate curve resolution [26], and very recently from measurements of thermal conductivity [27], in all instances in the very dilute alcohol regime. In particular, Raman experiments seem to suggest that tetrahedrality is enhanced in the hydration shell of water, due to the presence of clathrate-like structures [26]. Molecular dynamic simulations carried by Tan and coworkers [28] agree with this picture but show a considerable dependence on the choice of water model, being the SSDQO1 [29] the one that agrees best with the experiment. All these results seem to fit largely into the "iceberg model" picture of Franks and Evans. They provide an interpretation that might explain the rising TMDs feature, even though none of these works is addressing the specific problem directly.

So far, the attempts to explain the TMD anomaly enhancement of short chain alcohol solutions, either using simple phenomenological theories [13], two scale model simulations [19,21], or all-atom molecular dynamics calculations [20,22] are somewhat contradictory and far from satisfactory. Therefore, in this work we decided to address the problem with a model that is far more realistic than two-scale models, reproduces the geometry of the hydrogen bond network but lacks

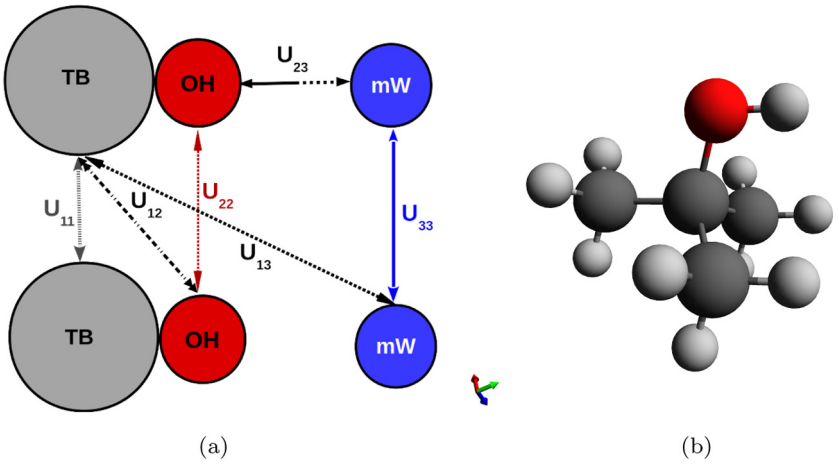

Fig. 1. (a) Our TBA and water models and their interactions. TB denotes the tert-butyl group (1), hydroxyl group is represented by the OH site (2), and mW indicates a one-site water molecule (3) modeled with the mW potential [30]. (b) All-atom pictorial representation of the tert-butyl alcohol molecule.

the complexity of all-atom models. Our model is inspired on the one proposed by Molinero and Moore [30] to account for the tetrahedral structure of liquid and solid water without explicitly accounting for hydrogen atoms. To that aim these authors resorted to the use of a Stillinger–Weber potential, which is characterized by the presence of a strongly directional three-body component that favors tetrahedral coordination [31]. Our alcohol of choice is tert-butanol. Its water solutions present of marked thermodynamic anomalies [32,33]. Among them, highly diluted tert-butanol solutions exhibit the most significant increase of the TMD among all short chain alcohols. It is the highest molecular mass alcohol to be completely miscible with water in all proportions under ambient conditions, and its bulky tert-butyl group doubtless epitomizes the effects of hydrophobic hydration. A possible origin of this anomalous behavior of alcohols in water has already been attributed to the formation of clathrate-hydrates [34], which fits well within the "iceberg model" picture and the Raman spectra results of Davis et al. [26] for ethanol/water solutions. In this way, thanks to the interplay between hydrogen bonding (which guarantees solubility and an enhancement of ice-like structures), and large hydrophobic effects (due to the bulky t-butyl tail) it can be understood why t-butanol solutions are the best candidates to display a visible TMD increase for low (but non-zero) alcohol concentration. Thus, one of the main goals of this work is to provide a model for tert-butanol alcohol (TBA) that qualitatively reproduces some of its main experimental properties (density, vaporization enthalpy). Once the TBA model is defined, the cross interaction parameters between the dimer and the water model (hereafter denoted by mW) are defined to qualitatively reproduce the behavior of the experimental excess molar volume and enthalpy.

Using extensive Molecular Dynamics (MD) simulations, we will show that our simple model captures the increase of the TMD of water upon addition of small amounts of TBA. In order to provide a microscopic picture of the hydration process, we have performed a local structure analysis for a series of temperatures above, at and below the TMD using Nguyen and Molinero's CHILL+ algorithm [35]. This algorithm allows for an identification and quantification of ice like, clathrate, and liquid like structures in a series of configurations of water molecules. This analysis was run on configurations of our dimer TBA model solution and of the all atom flexible model of Ref. [22]. In this way, we have been able to provide a correlation between the structural reorganization of water due to the presence of TBA molecules and the corresponding changes in the TMD. Also, one can get some insight as to why the all-atom alcohol/water models previously studied [20,22] do not seem capable of reproducing the subtle effects that the presence of alcohols have on the density anomaly.

The rest of the paper is organized as follows. In Section 2 we introduce our models for water and TBA and the simulation details. In Section 3 we present our most significant results and comment on them. The paper is closed by a brief summary and an outline of our main conclusions.

2. Model and simulation details

Our model coarse-grains the three water molecule atoms into a single site, the mW model, and the fifteen TBA atoms to our two site model, as depicted in Fig. 1(a) in which all the interactions involved are indicated by straight lines. In order to denote the pair site–site interactions, sites are labeled as follows: tert-butyl (TB) as 1, hydroxyl (OH) as 2 and water as 3.

Table 1
Parameters of the water–water interactions represented by the Moore and Molinero [30] model.

Water–water interaction parameters					
ϵ	σ	a	λ	γ	$cos(\theta_0)$
6.189	2.3925	1.80	23.15	1.20	−0.3333333
A		B		p	q
7.049556277		0.6022245584		4.0	0.0

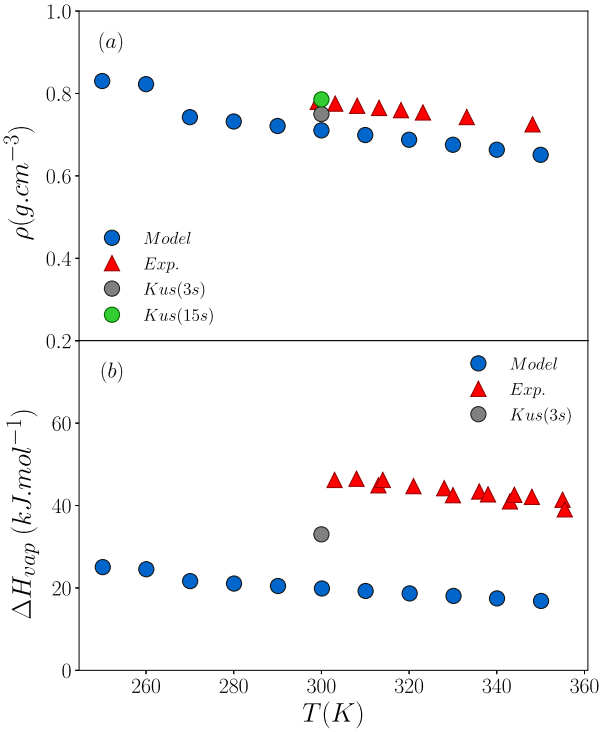

Fig. 2. (a)Density and (b)vaporization enthalpy of our model in comparison with experimental data [37] and Kusalik models. 3s refers to the 3-site united atom model, and 15 s to the fully atomic 15-site one [38,39].

2.1. Water model

First, for describing the single site water molecule we employ the mW model [30]. It was devised to tune Stillinger–Weber's potential, originally designed for Silicon [31], to reproduce a collection of macroscopic properties of water, preserving the tetrahedral coordination of oxygen atoms in ice [36]. The model is a coarse-grained representation of water molecules in which only effective oxygen–oxygen interactions are accounted for. It has two- and three-body contributions of the form

$$U_{33}(r) = \sum_i \sum_{j>i} \phi_2(r_{ij}) + \sum_i \sum_{j\neq i} \sum_{k>j} \phi_3(r_{ij}, r_{ik}, \theta_{ijk}), \tag{1}$$

where

$$\phi_2(r) = A\epsilon \left[B\left(\frac{\sigma}{r}\right)^p - \left(\frac{\sigma}{r}\right)^q\right] \exp\left(\frac{\sigma}{r - a\sigma}\right), \tag{2}$$

and

$$\phi_3(r, s, \theta) = \lambda\epsilon \left[\cos(\theta) - \cos(\theta_0)\right]^2 \exp\left(\frac{\gamma\sigma}{r - a\sigma}\right) \exp\left(\frac{\gamma\sigma}{s - a\sigma}\right). \tag{3}$$

The corresponding mW parameters are collected in Table 1. The potential parameters were fitted to reproduce the most significant structural and thermodynamic features of water. On the downside, it over-predicts the amount of tetrahedral order, has a lower melting point and TMD than experimentally measured.

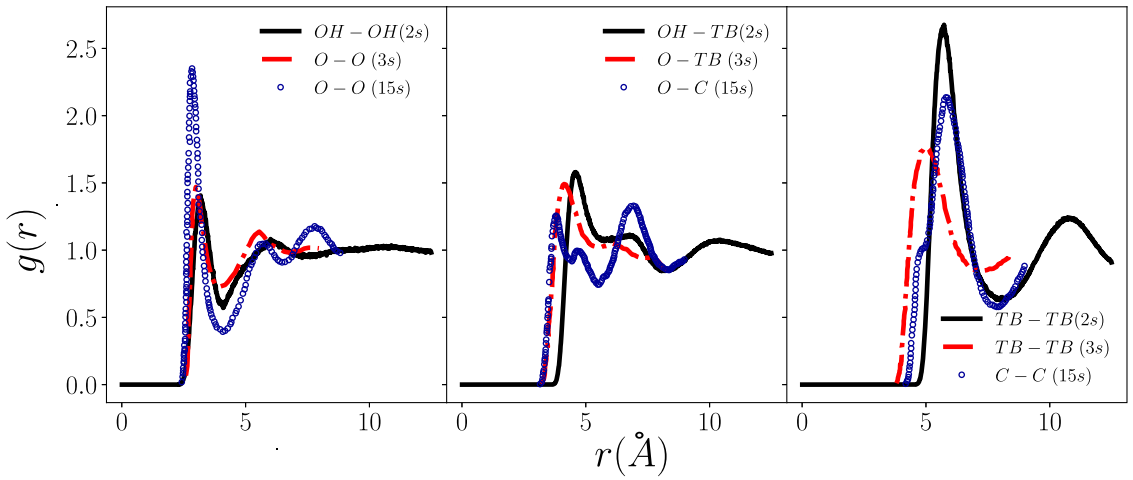

Fig. 3. Comparison between radial distribution function from our two-site model and Kusalik et al. two atomistic models for tert-butanol: 3-site [38] and 15-site [39].

Table 2
Site–site parameters for TBA–TBA interactions. Cross interaction parameters are computed using the standard Lorentz–Berthelot (LB) combining rules. In the case of OH–OH, all remaining parameters retain the original values of Moore and Molinero [30] found in Table 1.

TBA–TBA interaction parameters						
OH–OH interactions					TB–TB interactions	
ϵ (kcal/mol)	σ (Å)	λ	γ	p	ϵ (kcal/mol)	σ (Å)
1.50	2.60	65.00	1.2	5	0.25	5.45
TB-OH interactions						
$\epsilon(kcal/mol)$				σ(Å)		
0.61				4.03		

2.2. Tert-butanol model

The tert-butanol molecule illustrated in Fig. 1(b) is coarse-grained into a two site model: an apolar tert-butyl site which interacts via a Lennard-Jones potential, U_{11}, with the TB site of other molecules and the hydroxyl group which interacts through a Lennard-Jones potential with TB site of other molecules, U_{12}, and with other OH sites via a Stillinger–Weber potential similar to the mW interaction, U_{22}, in which the three-body terms will account for the hydrogen bonding. In addition, a tert-butyl site will be placed 1.836 Å apart from the hydroxyl, building a dimer molecule. This distance is taken from the geometry parameters of Kusalik et al. three-site model [38]. The whole set of parameters are tuned to reproduce qualitatively the experimental density and vaporization enthalpies, at least to a comparable level as those of the atomistic models of Kusalik et al. [38,39], shown in Fig. 2, and the radial distribution functions obtained for the three-site and fifteen-site models of Kusalik and coworkers [38,39], as depicted in Fig. 3. Cross interaction parameters are calculated with the standard Lorentz–Berthelot combination rules. LJ potentials are truncated at 12.5 Å and long range corrections to the energy and pressure are applied.

The final set of parameters is collected in Table 2. Fig. 2(a) shows that our model for the tert-butanol performs reasonably well for the density when compared with the experiments. Actually it presents less than ten percent deviation from the experimental values which compares reasonably well with the four percent departure of the more sophisticated three site model of Ref. [38]. In particular the temperature dependence is correctly reproduced. Deviations in the vaporization enthalpy shown in Fig. 2(b) are substantially larger when our results are compared with experiments, but in our opinion, given that even a more sophisticated model (such as the three-site model by Kusalik et al.) could not reproduce the experimental value of the vaporization enthalpy at $T = 300$ K, the discrepancy found in our two-site-model seems perfectly acceptable. Note that even for sophisticated water models, vaporization enthalpy is only reproduced when a term to account for the different self-polarization of liquid water are introduced ad hoc [40].

The analysis of the pair distribution functions presented in Fig. 3 shows that the agreement with the atomistic models is reasonable, being our model logically closer to the three site model when compared with the fifteen site model. This is specially so for the OH–OH and OH–TB partial distributions. Differences between the fifteen site, three site and our model are in any case significant. Not surprisingly, the 15-site model yields pair distribution functions that seem to be in better qualitative agreement with experimental results from neutron diffraction [42]. As to hydrogen bonding, our model gives a

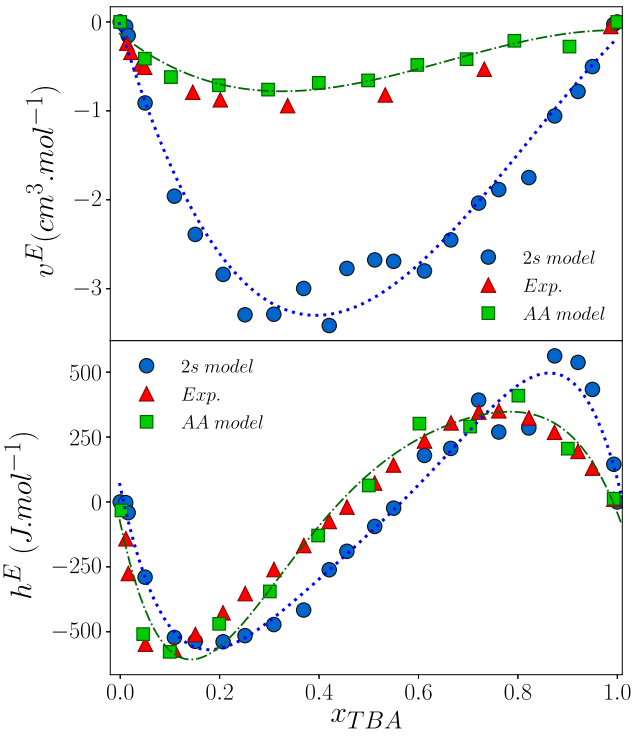

Fig. 4. Experimental (red) [41], Full-atom model [22] (green) and our model's (blue) excess thermodynamic properties of TBA/water solutions: excess volume (top) and excess enthalpy (bottom).

coordination number from the integration of g_{OH-OH} up to its first minimum of 2.07 hydrogen bonds, which is somewhat larger than the values 1.62 and 1.77 of Kusalik et al. for three site and 15 site models respectively [38]. Experimental estimates lie in the range from 1.4 to 1.8 [42]. Note that the somewhat stronger hydrogen bonding of our model is due to the large value of the λ-parameter (cf. Table 2). Although it is to some extent compensated by the smaller ϵ, it is substantially larger that of water. This however was necessary to keep the density down to the approximate experimental value, while at the same time keeping the system in the liquid state at 1 bar in the range from room temperature down to the TMD and a bit below. We will see later this has consequences for the fit of the mixture parameters.

2.3. Water/tert-butanol solution model

Next, the tert-butyl/water interaction (U_{13}) is modeled via a plain LJ potential truncated at 12.5 Å with long range corrections to the energy and pressure are applied. The OH-water interaction (U_{23}) is again a Stillinger–Weber potential with a three-body component, for which the ϵ and σ parameters have been optimized.

These parameters are fixed in terms of excess quantities. The excess quantity is the difference between the value of a given property of the mixture and the corresponding value calculated from those the pure solute and solvent in an ideal mixture. As shown in Ref. [20], excess properties from simulated models can hardly be reproduced if the cross interactions between different molecular components are computed using standard mixing rules. The obvious route to bypass this shortcoming is to adjust these cross interaction parameters to fit the experimental value of the excess properties over the whole composition range. In our case we have used as reference quantities to be fitted the excess enthalpy [43] and excess volume [41]. Given the large value of the λ parameter for TBA–TBA interactions, it seemed at first sensible to use $\lambda_{OH-mW} = \sqrt{\lambda_{OH-OH}\lambda_{mW}}$. This choice however, led to a TMD that decreased monotonously with TBA concentration. For this reason, we decided to keep the value for the hydrogen bond interaction between the hydroxyl group of the TBA and water exactly the same as that of pure water, that is, $\lambda_{OH-mW} = 23.15$. We then proceeded to adjust the remaining parameters to the excess properties.

Results from the fit are illustrated in Fig. 4, and we can see that the model reproduces qualitatively the experimental behavior, both the volume contraction and the non-monotonic compositional dependence of the excess enthalpy, although not as well as the full-atom model [22]. The final fitted parameters are collected in Table 3.

A snapshot of a configuration for $x_{TBA} = 0.005$ and 252 K along a molecular dynamics trajectory, is depicted in Fig. 5. Dimers correspond to TBA molecules, and spheres to water molecules color-coded depending on the geometry of their individual local environment following the classification introduced by Nguyen and Molinero [35] (see Section 3.2 below

Table 3
Optimal cross interaction parameters for our TBA–water mixture model. In the case of OH–mW, all remaining parameters take the original values of Moore and Molinero [30] found in the Table 1.

TBA–water interaction parameters			
TB–mW interactions		OH–mW interactions	
ϵ (kcal/mol)	σ (Å)	ϵ (kcal/mol)	σ (Å)
0.459	3.984	1.371	3.660

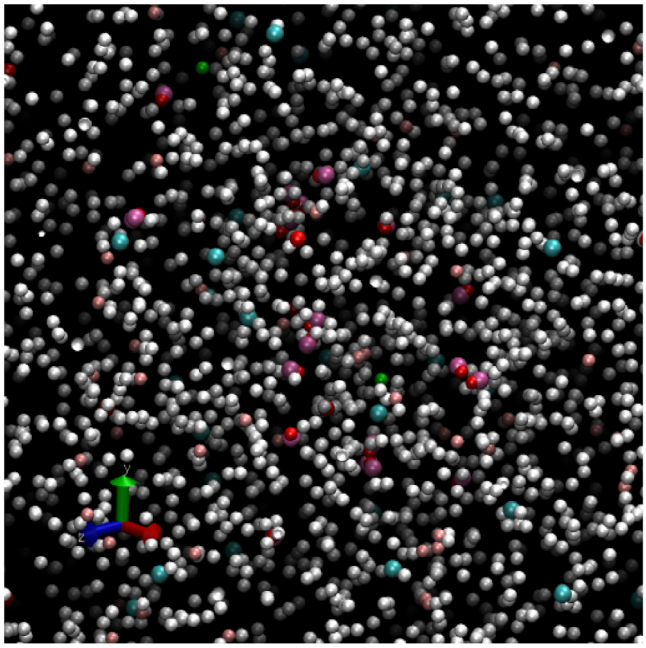

Fig. 5. Snapshot of a configuration of TBA (red–violet dimers) in water for $x_{TBA} = 0.005$ and T=252 K. Spheres of different colors correspond to water molecules in different local environments according to the CHILL+ classification [35], namely liquid-like (white), cubic ice-like (blue), hexagonal ice-like (green), clathrate-like (red), interstitial clathrate (pink) and interfacial ice-like (cyan).

for a more detailed description of the structural analysis). What it is immediately apparent from the snapshot is that alcohol molecules have certain tendency to aggregate, basically driven by their strong H-bonds. Nonetheless, some free TBA molecules are visible and throughout the whole composition range the system does not phase separate. As found by Kežić and Perera [44], all-atom models of TBA aqueous solutions also display a tendency to microsegregate, without reaching a complete phase separation (which is also absent in real TBA solutions).

2.4. Simulation details

Employing the water and tert-butanol models described above we performed MD simulations for a number of systems with particle numbers ranging from 2000 (pure water) to 4000 (pure TBA) for various compositions using the LAMMPS package [45]. Simulations were performed in the isothermal–isobaric ensemble with a Nosé-Hoover thermostat and barostat [46,47] with a time-step of one fs and relaxation times of 10ps and 100ps respectively. Particles were placed in a cubic box with standard periodic boundary condition. The dimer bonds were kept fixed using a SHAKE algorithm [48], with a tolerance factor of 10^{-4}. Our simulations started from a compositionally disordered mixture of TBA and water particles, which was equilibrated at the chosen pressure and temperature for 2 ns. Production runs were 10 ns long.

To ensure that the system was thermalized, the evolution of the pressure, and the kinetic and potential energies were closely monitored during the equilibration run. Configurations were stored every 2 ps and running averages computed every 0.1 ps. Additionally, we have run all-atom simulations using an optimized OPLS-AA model proposed by Jorgensen et al. [49] in combination with a TIP4P/2005f flexible model for water [23] and cross interaction parameters fitted to experimental excess properties [22]. Simulations for pure TIP4P/2005f water were also run. Here we have used the GROMACS package [50,51] in the isothermal–isobaric ensemble with a time-step of 0.5 fs. Configurations were stored every 2000 time-steps for temperatures approximately at the TMD and some 10 K above and below, in order to analyze the structural changes taking place when crossing the temperature of maximum density at constant pressure.

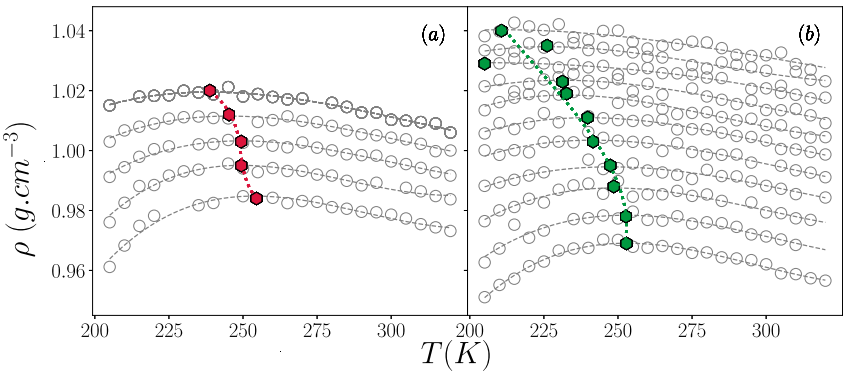

Fig. 6. Density isobars for pressures (a) 1 bar, 500 bar, 1000bar,...,2000bar (from bottom to top) for TBA in water with $x_{TBA} = 0.005$ and (b) 1 bar, 500 bar, 1000bar,...,5000bar with $x_{TBA} = 0.01$. Simulation data are denoted by symbols and lines correspond to a third degree polynomial fit.

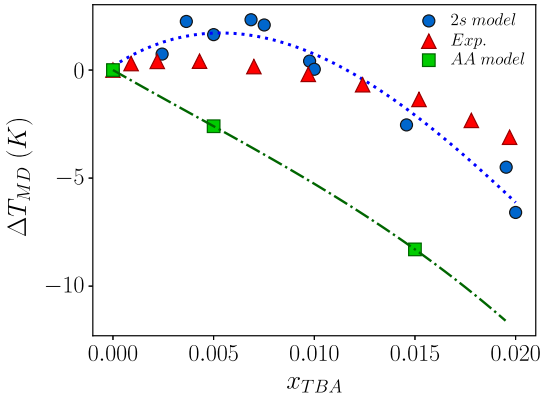

Fig. 7. Mole fraction dependence of the change in the TMD of water/TBA solutions with respect to that of pure water. Blue circles correspond to our model results, green squares to full-atom model [22], and red triangles denote experimental data [41]. The dashed lines are an eye-guide.

3. Results and discussion

Fig. 6 illustrates density isobars for the water–TBA mixture for various pressures and TBA mole fractions $x_{TBA} = 0.005$ and $x_{TBA} = 0.01$. The dashed curves correspond to third degree polynomial fits. With these fits we obtained the temperature of maximum density denoted by filled pentagons in the graph. As the pressure grows, the TMD decreases in agreement with experimental findings [40]. We observe this behavior for all the mole fractions studied. The origin of the decrease of the temperature of maximum density due to pressure increase can be attributed to the fact that pressure tends to hinder the formation of low density ice-like and clathrate structures by which the anomalous region of water (or water solutions here) is shifted to lower temperatures. The change in the TMD due to the addition of solute, $\Delta T_{MD}(x_{TBA})$, is a key quantity not only to test if the model reproduces the experiments but also to understand the mechanism behind the unusual increase of the excess of temperature of maximum density with the addition of solute. Fig. 7 compares the ΔT_{MD} versus TBA concentration obtained by our simulations with experiments by de Wada and Umeda [2]. Our model gives the maximum of $\Delta T_{MD}(x_{TBA}) \sim 2$K, for a TBA fraction $x_{TBA} \sim 0.005$ which is approximately the TBA fraction corresponding to the maximum ΔT_{MD} in the experiments. It is readily apparent that our model overestimates the maximum increase of the TMD. For higher TBA concentrations, the curve reaches $\Delta T_{MD}(x_{TBA}) < 0$ for $x_{TBA} \gtrsim 0.01$, a value slightly higher than that of the experimental crossover. For even larger values of x_{TBA}, the excess TMD decreases further, as it does experimentally, up to a point where it is either destroyed (TBA does not exhibit any density anomaly) or preempted by crystallization.

One possible reason for the overestimated value of the maximum $\Delta T_{MD}(x_{TBA})$ is that our model is endowed with stronger hydrogen bonds between TBA molecules than those between water molecules. This effect promotes the formation of TBA clusters with large hydrophobic surfaces. In turn this might enhance the increase in the temperature of maximum density due to the enlargement of the hydrophobic hydration shell.

3.1. Partial molar volume analysis

The solute's partial molar volume dependence on temperature and concentration are known to be related to the changes in the TMD (e.g. see Eqs.(24)-(27) in Ref. [7]). This means that a further consistency check of our results can be

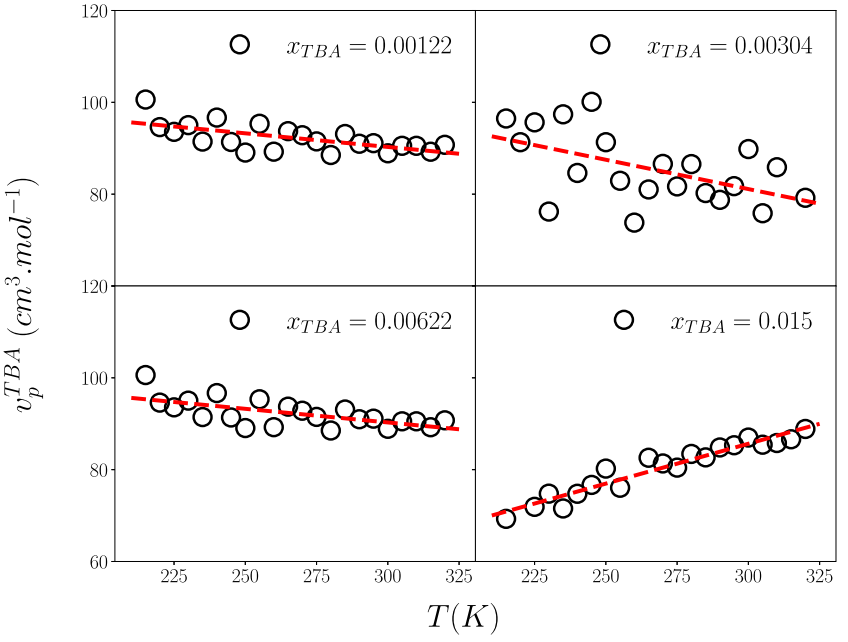

Fig. 8. TBA partial molar volume v_p^{TBA} plotted as a function of temperature T for four TBA mole fractions x_{TBA} at dilute regime. Dashed red lines indicate the slopes obtained by least squares fit.

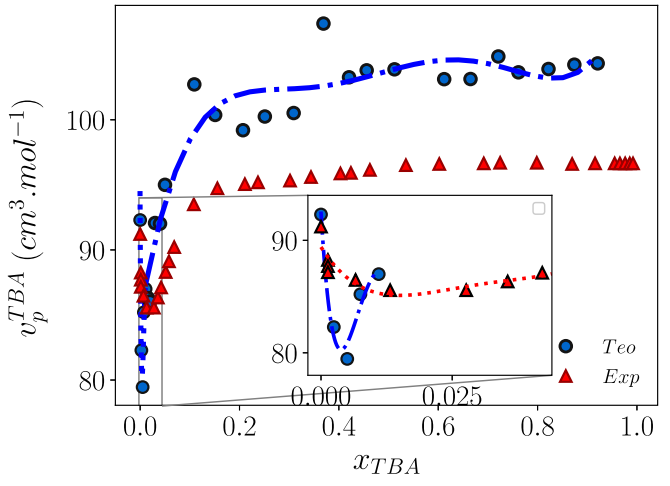

Fig. 9. The partial molar volumes of TBA as a function of mole fraction x_{TBA}. The derivatives were estimated by a numerical difference. Red triangles are experimental data from [41].

obtained through their analysis. The relation between TBA partial molar volume, v_p^{TBA}, and molar volume of the mixture v is described by [52,53]

$$v_p^{TBA} = v + (1 - x_{TBA}) \left(\frac{\partial v}{\partial x_{TBA}} \right)_{p,T}, \tag{4}$$

that can be expressed at low TBA concentrations using the incremental method [54,55] as follows:

$$v_p^{TBA}(x_{TBA}) = \frac{v(x_{TBA} + \Delta x_{TBA}) + v(x_{TBA} - \Delta x_{TBA})}{2} + (1 - x_{TBA}) \times \frac{v(x_{TBA} + \Delta x_{TBA}) - v(x_2 - \Delta x_{TBA})}{2\Delta x_{TBA}}. \tag{5}$$

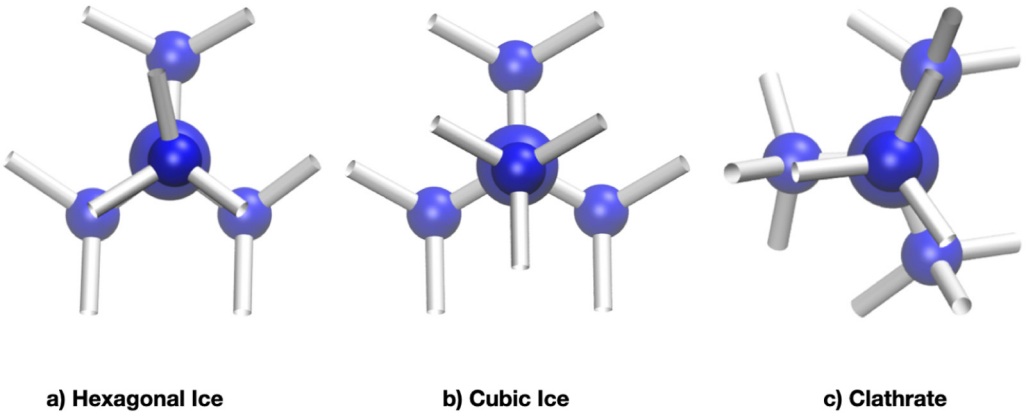

Fig. 10. Local structures corresponding to ice an clathrate water in bulk. The corresponding interfacial structures have one missing bond. See the text for a description in terms of eclipsed and staggered bonds.

We identify the terms of the interval $(x_{TBA} - \Delta x_{TBA}, x_{TBA} + \Delta x_{TBA})$ with two consecutive TBA mole fractions. The small difference between consecutive mole fractions makes this method suitable. Fig. 8 shows the behavior of v_p^{TBA} with the temperature for four TBA mole fractions around the value of x_{TBA} for which ΔT_{MD} is maximum. It shows that only for the highest mole fraction analyzed, $x_{TBA} = 0.015$, v_p^{TBA} increases with temperature. As the mole fraction decreases below $x_{TBA} = 0.015$, the slope of the curve v_p^{TBA} changes sign (i.e. $\left(\partial v_p^{TBA}/\partial T\right)_P < 0$), indicating the occurrence of the maximum in the ΔT_{MD} close to $x_{TBA} = 0.005$. Fig. 9 compares the behavior of v_p^{TBA} versus x_{TBA} at 300 K for our model and experimental results [41]. The figure shows that there is a qualitative agreement between our results and the experimental data. Both exhibit a drop in the partial volume of TBA as the concentration decreases at very low TBA mole fractions. In our case, however, the decrease occurs at a higher dilution regime ($x \sim 0.005$), which coincides with the maximum we have obtained in the TMD variation (ΔT_{MD}). Such drop beginning from infinite dilution in the partial molar volume with increasing concentration has been observed experimentally and in simulations of water–alcohol mixtures [7,28,56,57].

3.2. Structural analysis

In summary, our simple model of short chain alcohol displays the "structure maker" character observed experimentally, i.e. a solute that increases the temperature of the maximum density of water. In order to correlate the non-monotonic density dependence of water and water/TBA with microscopic structural changes, we have analyzed a series of configurations from our TBA/water model using Nguyen and Molinero's CHILL+ algorithm [35]. This procedure allows for the identification and quantification of local structures of water molecules depending on the number and configuration of their nearest neighbor bonds. Depending on their relative disposition, bonds are classified as eclipsed and staggered. Then, the algorithm identifies cubic ice-like structures, (no eclipsed and four staggered bonds), hexagonal ice-like, (one eclipsed and three staggered bonds), interfacial ice-like structures, (any number of eclipsed bonds and 2 or 3 staggered bonds), interfacial clathrate-like structures, (three eclipsed and any number of staggered bonds), and finally clathrate like structures, (four eclipsed bonds and no staggered bonds). See Fig. 10 for a graphic representation of solid-like and clathrate local structures. Note that interfacial structures are derived from those depicted by removing one of the bonds. All other local structures with higher coordinations are cast into the class of liquid-like particles. In any case, it is worth noticing that the lowest density structures correspond to ice-like and clathrates, are all tetrahedrally coordinated. Since the latter corresponds to distorted tetrahedra, they will lead to a slightly higher density: a network of perfect tetrahedra will always yield a more open (less dense) structure. We will see how this is reflected in the TMD. For the sake of comparison we will also perform the same kind of analysis on our own first tentative model with stronger OH–mW interactions, and on the more sophisticated model for water/TBA mixtures with flexible all-atom potentials proposed in Ref. [22]. Both models are unable to reproduce the TMD increase upon TBA addition, and consequently the analysis performed using CHILL+ will illustrate the key differences between models at the microscopic level.

Figs. 11 show the histograms of relative abundance of local clathrate hydrates (Ct), hexagonal ice (HI), cubic ice (CI), interfacial clathrates (ICt), interfacial ice (II), and liquid water (L) for five models: mW [30] and flexible TIP4P/2005f [23] pure water models – upper graphs – and flexible all-atom TIP4P/2005f-OPLS model of [22] and our TBA/mW model and its variation with stronger water–TBA H-bonding — lower graphs. Statistical uncertainties are not visible at the scale of the figure.

Focusing first on pure water models, we observe in the upper graphs of Figs. 11 that only clathrate hydrate structures exhibit a subtle maximum at the TMD for both water models. In the case of the mW water model a maximum is also present in interfacial clathrate structures. Clathrate-like structures are tetra-coordinated oxygen atoms but with

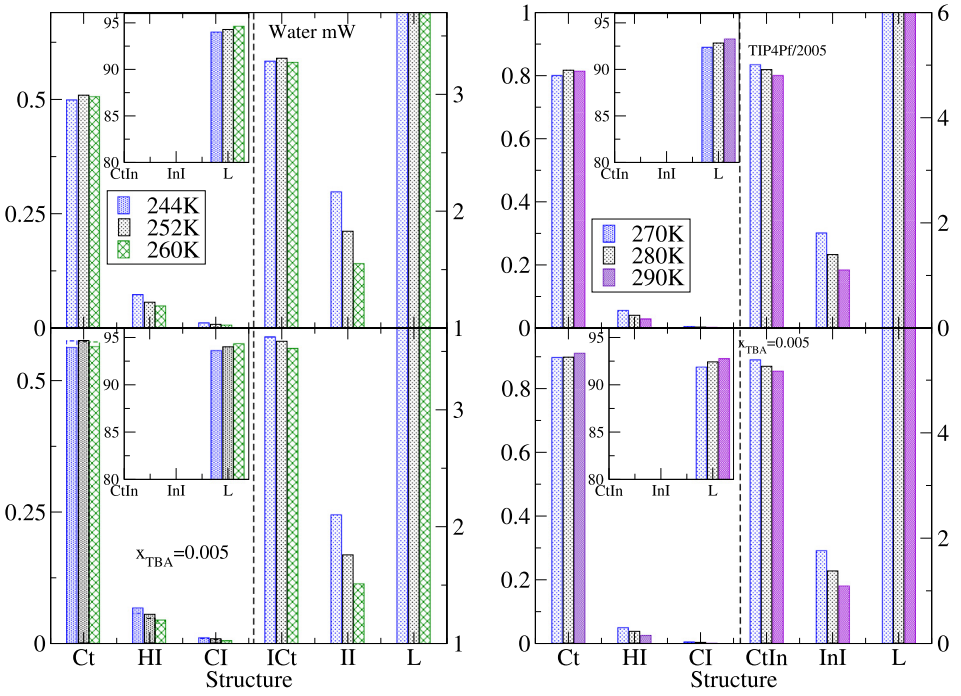

Fig. 11. Histograms of relative abundance of local clathrate hydrates (Ct), hexagonal ice (HI), cubic ice (CI), interfacial clathrates (ICt), interfacial ice (II), and liquid water (L), as determined using CHILL+ algorithm [35] on 2000 for (a) Pure mW water (upper graph) and mW water+our TBA model (lower graph). Dashed bars (visible mostly on the clathrate – Ct – data) correspond to our model with stronger OH–mW hydrogen bonds ($\lambda_{OH-mW} = 36$) (b) TIP4P/2005f pure water model (upper graph), and flexible all-atom TIP4P/2005f-OPLS [22] mixture models (lower graph). Notice the vertical dashed lines that separate data with ordinates on the left and right axis.

eclipsed bonds [35]. As temperature increases, both these and liquid-water structures grow initially at the expense of ice-like structures. Being almost perfectly tetrahedral, ice-like structures are less dense. This explains the initial anomalous increase of density. From the TMD onward, the relative weight of low density structures (clathrate, and ice-like structures both bulk and interface) diminishes considerably, and density decreases due to the regular thermal expansion of the high density liquid water structure.

Thus, the interplay between a small maximum in low density structures (clathrates) and increase of liquid-like (high density) structures seems to be at the source of the existence of a TMD. All other low density (ice-like) structures have a very small presence after melting, and display a monotonic decrease with increasing temperature. It is important to notice that the clathrate structures occur in both models of pure water, so its existence does not require – although, as shown below, it is enhanced by – the presence of solute molecules.

Next, in the case of the lower graphs of Fig. 11 we have the corresponding histograms for the solutions at $x_{TBA} = 0.005$, i.e. close to the maximum of $\Delta T_{MD}(x_{TBA})$ for our model. Our results exhibit again a maximum in the bulk clathrate hydrate structures. Interestingly the maximum does not occur for the interfacial clathrates anymore. In the solution, these structures are basically promoted by the presence of solute molecules, and their relative weight monotonically decreases with temperature. Now, in the TIP4P/2005f-OPLS model the maximum is shifted to temperatures well beyond the TMD, the region shown in the figure displaying a slight increase in the relative weight of the clathrate structures. Also, in our model with stronger water–TBA H-bonds the clathrate-like structures maximum has practically vanished. This implies that in these two cases, as temperature reaches the TMD the number of clathrate structures does not grow appreciably, and consequently the density increase from the melting temperature is smaller, by which $\Delta T_{MD} < 0$. For higher temperatures, above the TMD, the thermal expansion of the dominant liquid-like structures controls the temperature dependence of the density, and thus the water anomaly disappears.

Now, we may ask ourselves where one should expect to find the largest concentration of clathrate-like structures in the presence of TBA solute molecules. To answer this question, in Fig. 12 we have plotted the pair correlation function $g_{TB-Ct}(r)$ between tert-butyl sites and water molecules with a clathrate-like local environment. In the same graph we also include the corresponding r-dependent coordination number, n_{Tb-Ct}. For our model (black curves)we observe that the first coordination shell reaches up to 5.8 Å, which roughly corresponds to the first hydration shell ($r < 5.4$ Å) [24]. Interestingly, the effect extends moderately up to the second coordination layer, in contrast with the model with a modified stronger H-bonding between TBA and water (red curves). Looking at the integrated coordination numbers, one observes that in our model (which reproduces the experimental rise of the TMD) the number of clathrate like structures is slightly higher

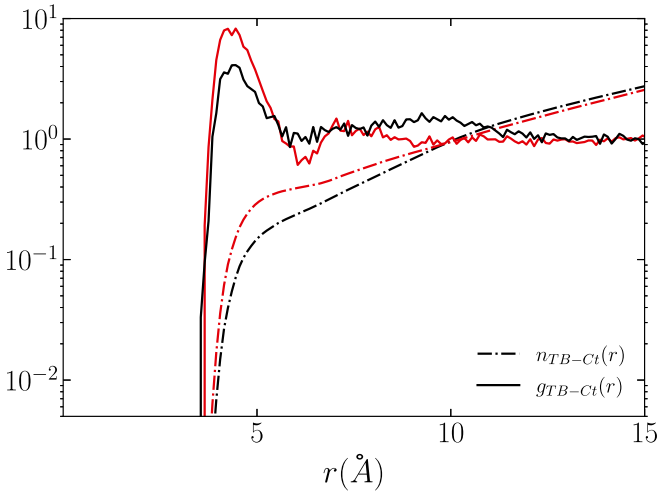

Fig. 12. Pair correlation functions (solid curves) between tert-butyl sites and water molecules with clathrate-like (Ct) local structures and corresponding integrated r-dependent coordination numbers (dashed curves). In black our present model for TBA-mW water, in red curves corresponding to the model with a stronger OH–mW hydrogen bonding.

since the effect propagates further into the bulk. The tendency of the TBA molecules to aggregate in our solution model leads to the formation of larger clusters with big hydrophobic surfaces and an overgrown hydration shell. This is likely the origin of the overestimation of ΔT_{MD} already commented upon in previous paragraphs.

Finally, in our model, for a larger concentration, such as $x_{TBA} = 0.02$ the density anomaly occurs at very low temperatures, where the large fluctuations in the results are connected with the onset of crystallization and $\Delta T_{MD}(x_{TBA}) < 0$. In this case, the solute behaves now as a strong "structure breaker". We have observed that the maximum in the ratio of bulk clathrate structures is much less marked. Also, the relative weight of interfacial clathrates increases 25 percent with respect to the value for pure water and diminishes with increasing temperature. As in the case of the all-atom model, these structures are promoted by the presence of solute molecules and their relative weight depends on the concentration of the latter. As discussed above, the decrease in the maximum of bulk clathrate structures is directly connected with the fall in the TMD. Larger increases in x_{TBA} will lower the TMD even further, and the density anomaly will be completely preempted by crystallization/vitrification. Apparently, in the all-atom model solution, the shift of the bulk clathrate structure maximum, and in our dimer TBA model the smoothing of the corresponding maxima for concentrations above $x_{TBA} \sim 0.01$ (or when the TBA–water H-bond is stronger that of bulk water), are the structural features that determine the "structure breaker" character of the solutes. For concentrations below $x_{TBA} \sim 0.01$, our model solute behaves as a "structure maker".

4. Summary and conclusions

In this paper we proposed a simple diatomic model for TBA with three body interactions on the hydroxyl site that mimic the formation hydrogen bonds. Cross interactions were fitted to qualitatively account for the experimental excess properties of water/TBA solutions, with water represented by Molinero and Moore's model [30]. This model is capable of reproducing the experimental enhancement of the density anomaly of water observed for very small concentrations of alcohol. A structural analysis of the simulation results illustrates the correlation between the presence of a maximum of clathrate-like structures and the density anomaly. The fact that the maximum occurs in the bulk clathrates and not interfacial clathrates and that high density liquid like structures also increase in a monotonic fashion with temperature seems to be at the root of the density anomaly enhancement. As found in Ref. [22], a much more sophisticated all-atom model is unable to reproduce the experimental behavior, and the same shortcoming is found here for our model when the TBA–water H-bond strength is increased. In both instances the maximum in the clathrate-like water structures disappears. This further supports the idea that the presence of this maximum is at the root of the TMD increase. It is important to notice that experimental works such as the spectroscopic analysis of Davis et al. [26] correlate the thermodynamic anomalies of alcohol solutions with the stiffening of the hydrogen bond network, which is in turn associated with the increase of clathrate-like structures in the hydration shell around the alkyl tails.

Finally, the failure of some models to reproduce the experimental TMD enhancement might be ascribed to their inability to adequately account for the alcohol–water H-bond interaction. This, as we have seen in our model, changes dramatically the structural behavior of the dilute solution. Also, Tan and coworkers [28] have shown that the choice of the water model is crucial for an accurate representation of the experimental results. An overall excellent model such as the TIP4Pf/2005 [23] might not necessarily be the best choice to account for the subtle changes induced in water by solutes at

high dilution. Under such conditions, alkyl groups are considerably polarized by the local field of the surrounding water molecules and this might lead to strong non-additive effects that must be taken into account. Further research in this direction is planned.

CRediT authorship contribution statement

Murilo S. Marques: Methodology, Data curation, Writing - original draft, Writing - review & editing. **Enrique Lomba:** Conceptualization, Methodology, Writing - original draft, Writing - review & editing, Supervision. **Eva G. Noya:** Software, Visualization, Validation. **Diego González-Salgado:** Conceptualization, Methodology, Software. **Marcia Barbosa:** Conceptualization, Methodology, Writing - original draft, Writing - review & editing, Supervision.

Declaration of competing interest

The authors declare that they have no known competing financial interests or personal relationships that could have appeared to influence the work reported in this paper.

Acknowledgments

EL, EGN and DGS acknowledge the support from the Agencia Estatal de Investigación and Fondo Europeo de Desarrollo Regional (FEDER) under grant No. FIS2017-89361-C3. MSM and MCB thanks the Brazilian science agencies - Conselho Nacional de Desenvolvimento Cientıfico e Tecnologico (CNPq) (INCT-Fc) and Coordenacão de Aperfeiçoamento de Pessoal de Nível Superior (CAPES Print Program) for the support to the collaborative period in the Instituto de Química Fisica Rocasolano. DG acknowledges to the Galicia Supercomputing Center (CESGA) for the computer time allocated for some of our calculations.

References

[1] A. Taffel, The temperature of maximum density of aqueous solutions, Trans. Faraday Soc. 19 (1923) 99, http://dx.doi.org/10.1039/tf9231900099.
[2] G. Wada, S. Umeda, Effects of nonelectrolytes on the temperature of the maximum density of water. I. Alcohols, Bull. Chem. Soc. Japan 35 (4) (1962) 646–652, http://dx.doi.org/10.1246/bcsj.35.646.
[3] G. Wada, S. Umeda, Effects of nonelectrolytes on the temperature of the maximum density of water. II. Organic compounds with polar groups, Bull. Chem. Soc. Japan 35 (11) (1962) 1797–1801, http://dx.doi.org/10.1246/bcsj.35.1797.
[4] F. Franks, The Physics and Physical Chemistry of Water, in: Franks, Felix, vol. 1, Springer US, 1972.
[5] P. Poole, F. Sciortino, U. Essmann, H. Stanley, Phase-behavior of metastable water, Nature 360 (1992) 324–328, http://dx.doi.org/10.1038/360324a0.
[6] M. Beretta, At the source of western science: The organization of experimentalism at the accademia del cimento (1657-1667), Notes Records Roy. Soc. London 54 (2) (2000) 131–151.
[7] H.S. Ashbaugh, H. Bukannan, Temperature, pressure, and concentration derivatives of nonpolar gas hydration: Impact on the heat capacity, temperature of maximum density, and speed of sound of aqueous mixtures, J. Phys. Chem. B 124 (31) (2020) 6924–6942, http://dx.doi.org/10.1021/acs.jpcb.0c04035, PMID: 32692557.
[8] H.S. Frank, M.W. Evans, Free volume and entropy in condensed systems III. Entropy in binary liquid mixtures; partial molal entropy in dilut e solutions; structure and thermodynamics in aqueous electrolytes, J. Chem. Phys. 13 (1945) 507, http://dx.doi.org/10.1063/1.1723985.
[9] A.J. Darnell, J. Greyson, Effect of structure-making and -breaking solutes on the temperature of maximum density of water, J. Phys. Chem. 72 (8) (1968) 3021–3025, http://dx.doi.org/10.1021/j100854a060.
[10] L.G. Hepler, Thermal expansion and structure in water and aqueous solutions, Can. J. Chem. 47 (24) (1969) 4613–4617, http://dx.doi.org/10.1139/v69-762.
[11] N. Galamba, Water's structure around hydrophobic solutes and the iceberg model, J. Phys. Chem. B, 117 (2013) 2153–2159, http://dx.doi.org/10.1021/jp310649n.
[12] N. Bignell, Partial molar volumes of atmospheric gases in water, J. Phys. Chem. 88 (22) (1984) 5409–5412, http://dx.doi.org/10.1021/j150666a060.
[13] S. Chatterjee, H.S. Ashbaugh, P.G. Debenedetti, Effects of nonpolar solutes on the thermodynamic response functions of aqueous mixtures, J. Chem. Phys. 123 (16) (2005) 164503, http://dx.doi.org/10.1063/1.2075127.
[14] K. Kasraian, P. DeLuca, Thermal analysis of the tertiary butyl alcohol-water system and its implications on freeze-drying, Pharm. Res. 12 (4) (1995) 484–490, http://dx.doi.org/10.1023/a:1016233408831.
[15] F. Franks, B. Watson, Maximum density effects in dilute aqueous solutions of alcohols and amines, Trans. Faraday Soc. 63 (1967) 329–334, http://dx.doi.org/10.1039/TF9676300329.
[16] T. Lilley, S. Murphy, The temperature of maximum density of aqueous electrolyte solutions and its relation to the temperature derivative of the partial molar volume of the solute, J. Chem. Thermodyn. 5 (4) (1973) 467–470, http://dx.doi.org/10.1016/S0021-9614(73)80092-8.
[17] D. Macdonald, B. Dolan, J. Hyne, The influence of substituted alcohols on the temperature of maximum density of water, J. Solution Chemistry 5 (1976) 405–416, http://dx.doi.org/10.1007/BF00646415.
[18] E.S. Kim, K.N. Marsh, Excess volumes for 2-methyl-2-propanol + water at 5 k intervals from 303.15 to 323.15 k, J. Chem. Eng. Data 33 (3) (1988) 288–292, http://dx.doi.org/10.1021/je00053a020.
[19] Z. Su, S.V. Buldyrev, P.G. Debenedetti, P.J. Rossky, H.E. Stanley, Modeling simple amphiphilic solutes in a Jagla solvent, J. Chem. Phys. 136 (2012) 044511, http://dx.doi.org/10.1063/1.3677185.
[20] D. González-Salgado, K. Zemánková, E.G. Noya, E. Lomba, Temperature of maximum density and excess thermodynamics of aqueous mixtures of methanol, J. Chem. Phys. 144 (18) (2016) 184505, http://dx.doi.org/10.1063/1.4948611.
[21] A.P. Furlan, E. Lomba, M.C. Barbosa, Temperature of maximum density and excess properties of short-chain alcohol aqueous solutions: A simplified model simulation study, J. Chem. Phys. 146 (14) (2017) 144503, http://dx.doi.org/10.1063/1.4979806.
[22] E.G. a Perez, D. González-Salgado, E. Lomba, Molecular dynamics simulations of aqueous solutions of short chain alcohols. Excess properties and the temperature of maximum density, Fluid Phase Equilib. 528 (2020) 112840, http://dx.doi.org/10.1016/j.fluid.2020.112840.

[23] M.A. González, J.L.F. Abascal, A flexible model for water based on TIP4p/2005, J. Chem. Phys. 135 (2011) 224516.
[24] H.S. Ashbaugh, J.W. Barnett, A. Saltzman, M.E. Langrehr, H. Houser, Stiffening of dilute alcohol and alkane mixtures with water, J. Chem. Phys. 145 (2016) 201102, http://dx.doi.org/10.1063/1.4971205.
[25] Y.L.A. Rezus, H.J. Bakker, Observation of immobilized water molecules around hydrophobic groups, Phys. Rev. Lett. 99 (2007) 148301, http://dx.doi.org/10.1103/physrevlett.99.148301.
[26] J.G. Davis, K.P. Gierszal, P. Wang, D. Ben-Amotz, Water structural transformation at molecular hydrophobic interfaces, Nature 491 (7425) (2012) 582–585, http://dx.doi.org/10.1038/nature11570.
[27] C. López-Bueno, M. Suárez-Rodríguez, A. Amigo, F. Rivadulla, Hydrophobic solvation increases thermal conductivity of water, Phys. Chem. Chem. Phys. (2020) http://dx.doi.org/10.1039/d0cp03778h.
[28] M.-L. Tan, J.R. Cendagorta, T. Ichiye, Effects of microcomplexity on hydrophobic hydration in amphiphiles, J. Am. Chem. Soc. 135 (13) (2013) 4918–4921, http://dx.doi.org/10.1021/ja312504q, PMID: 23506339.
[29] J.A. Te, T. Ichiye, Understanding structural effects of multipole moments on aqueous solvation of ions using the soft-sticky dipole–quadrupole–octupole water model, Chem. Phys. Lett. 499 (4–6) (2010) 219–225, http://dx.doi.org/10.1016/j.cplett.2010.09.043.
[30] V. Molinero, E.B. Moore, Water modeled as an intermediate element between carbon and silicon, J. Phys. Chem. B 113 (13) (2009) 4008–4016, http://dx.doi.org/10.1021/jp805227c, PMID: 18956896.
[31] F.H. Stillinger, T.A. Weber, Computer simulation of local order in condensed phases of silicon, Phys. Rev. B 31 (1985) 5262–5271, http://dx.doi.org/10.1103/PhysRevB.31.5262.
[32] D. Subramanian, M.A. Anisimov, Resolving the mystery of aqueous solutions of tertiary butyl alcohol, J. Phys. Chem. B 115 (29) (2011) 9179–9183, http://dx.doi.org/10.1021/jp2041795, PMID: 21671661.
[33] F. Aman-Pommier, C. Jallut, Excess specific volume of water + tert-butyl alcohol solvent mixtures: Experimental data, modeling and derived excess partial specific thermodynamic quantities, Fluid Phase Equilib. 439 (2017) 43–66, http://dx.doi.org/10.1016/j.fluid.2017.02.002.
[34] R. Kay, The Physical Chemistry of Aqueous Systems: A Symposium in Honor of Henry S. Frank on His Seventieth Birthday, Springer US, 2012.
[35] A.H. Nguyen, V. Molinero, Identification of clathrate hydrates, hexagonal ice, cubic ice, and liquid water in simulations: the CHILL+ algorithm, J. Phys. Chem. B 119 (29) (2014) 9369–9376, http://dx.doi.org/10.1021/jp510289t.
[36] V. Molinero, S. Sastry, C.A. Angell, Tuning of tetrahedrality in a silicon potential yields a series of monatomic (metal-like) glass formers of very high fragility, Phys. Rev. Lett. 97 (2006) 075701, http://dx.doi.org/10.1103/PhysRevLett.97.075701.
[37] National Institute of Standard and Technology, 2-propanol, 2-methyl, 2018, https://webbook.nist.gov/cgi/cbook.cgi?ID=C75650&Mask=4.
[38] P.G. Kusalik, A.P. Lyubartsev, D.L. Bergman, A. Laaksonen, Computer simulation study of tert-butyl alcohol. 1. Structure in the pure liquid, J. Phys. Chem. B 104 (40) (2000) 9526–9532, http://dx.doi.org/10.1021/jp001886w.
[39] P.G. Kusalik, A.P. Lyubartsev, D.L. Bergman, A. Laaksonen, Computer simulation study of tert-butyl alcohol. 2. Structure in aqueous solution, J. Phys. Chem. B 104 (40) (2000) 9533–9539, http://dx.doi.org/10.1021/jp001887o.
[40] H.L. Pi, J.L. Aragones, C. Vega, E.G. Noya, J.L. Abascal, M.A. Gonzalez, C. McBride, Anomalies in water as obtained from computer simulations of the TIP4p/2005 model: density maxima, and density, isothermal compressibility and heat capacity minima, Mol. Phys. 107 (2009) 365–374, http://dx.doi.org/10.1080/00268970902784926.
[41] G.I. Egorov, D.M. Makarov, Densities and volume properties of (water+tert-butanol) over the temperature range of (274.15 to 348.15)k at pressure of 0.1MPa, J. Chem. Thermod. 43 (3) (2011) 430–441, http://dx.doi.org/10.1016/j.jct.2010.10.018.
[42] D.T. Bowron, J.L. Finney, A.K. Soper, The structure of pure tertiary butanol, Mol. Phys. 93 (4) (1998) 531–543, http://dx.doi.org/10.1080/002689798168871.
[43] Y. Koga, Excess partial molar enthalpies of water in water-tert-butanol mixtures, Canadian J. Chem. 66 (12) (1988) 3171–3175.
[44] B. Kežić, A. Perera, Aqueous tert-butanol mixtures: A model for molecular-emulsions, J. Chem. Phys. 137 (1) (2012) 014501, http://dx.doi.org/10.1063/1.4730524.
[45] S. Plimpton, Fast parallel algorithms for short-range molecular dynamics, J. Comput. Phys. 117 (1) (1995) 1–19, http://dx.doi.org/10.1006/jcph.1995.1039.
[46] S. Nosé, A unified formulation of the constant temperature molecular dynamics methods, J. Chem. Phys. 81 (1) (1984) 511–519, http://dx.doi.org/10.1063/1.447334.
[47] W.G. Hoover, Canonical dynamics: Equilibrium phase-space distributions, Phys. Rev. A 31 (1985) 1695–1697, http://dx.doi.org/10.1103/PhysRevA.31.1695.
[48] J.-P. Ryckaert, G. Ciccotti, H.J. Berendsen, Numerical integration of the cartesian equations of motion of a system with constraints: molecular dynamics of n-alkanes, J. Comput. Phys. 23 (3) (1977) 327–341, http://dx.doi.org/10.1016/0021-9991(77)90098-5.
[49] W.L. Jorgensen, D.S. Maxwell, J. Tirado-Rives, Development and testing of the OPLS all-atom force field on conformational energetics and properties of organic liquids, J. Am. Chem. Soc. 118 (45) (1996) 11225–11236, http://dx.doi.org/10.1021/ja9621760.
[50] B. Hess, C. Kutzner, D. van der Spoel, E. Lindahl, GROMACS 4: Algorithms for highly efficient, load-balanced, and scalable molecular simulation, J. Chem. Theory Comput. 4 (2008) 435–447, http://dx.doi.org/10.1021/ct700301q.
[51] M.J. Abraham, T. Murtola, R. Schulz, S. Páll, J.C. Smith, B. Hess, E. Lindahl, GROMACS: High performance molecular simulations through multi-level parallelism from laptops to supercomputers, SoftwareX 1–2 (2015) 19–25, http://dx.doi.org/10.1016/j.softx.2015.06.001.
[52] J.S. Rowlinson, F.L. Swinton, Chapter 4 - The thermodynamics of liquid mixtures, in: J.S. Rowlinson, F.L. Swinton (Eds.), Liquids and Liquid Mixtures, third ed., in: Butterworths Monographs in Chemistry, Butterworth-Heinemann, 1982, pp. 86–131, http://dx.doi.org/10.1016/B978-0-408-24193-9.50008-4.
[53] A. Ben-Naim, Theory of solutions, in: Statistical Thermodynamics for Chemists and Biochemists, Springer US, Boston, MA, 1992, pp. 359–457, http://dx.doi.org/10.1007/978-1-4757-1598-9_6.
[54] C.A. Cerdeiriña, C.A. Tovar, D. González-Salgado, E. Carballo, L. Romaní, Isobaric thermal expansivity and thermophysical characterization of liquids and liquid mixtures, Phys. Chem. Chem. Phys. 3 (2001) 5230–5236, http://dx.doi.org/10.1039/B104891K.
[55] K. Zemanková, D. González-Salgado, E. Lomba, L. Romaní, Temperature of maximum density for aqueous mixtures of three pentanol isomers, J. Chem. Thermodyn. 113 (2017) 369–376, http://dx.doi.org/10.1016/j.jct.2017.07.011.
[56] M.-L. Tan, B.T. Miller, J. Te, J.R. Cendagorta, B.R. Brooks, T. Ichiye, Hydrophobic hydration and the anomalous partial molar volumes in ethanol-water mixtures, J. Chem. Phys. 142 (6) (2015) 064501, http://dx.doi.org/10.1063/1.4906750.
[57] H.S. Ashbaugh, J.W. Barnett, A. Saltzman, M. Langrehr, H. Houser, Connections between the anomalous volumetric properties of alcohols in aqueous solution and the volume of hydrophobic association, J. Phys. Chem. B 122 (13) (2018) 3242–3250, http://dx.doi.org/10.1021/acs.jpcb.7b08728, PMID: 28968101.